RJC

RASĀYAN *J. Chem.*
Vol. 17 | No. 1 |1-13| January - March | 2024
ISSN: 0974-1496 | e-ISSN: 0976-0083 | CODEN: RJCABP
http://www.rasayanjournal.com
http://www.rasayanjournal.co.in

NANO-DOPING EFFECT ON THE PROPERTIES OF LIQUID CRYSTALS BY USING COMPUTATIONAL APPROACHES

Sowmya Mudunuru[1], Chandra Sekhara Rao Gurubilli[1], Ganapavarapu Veera Raghava Sharma[1,✉], Srinivasa Rao G.[1] and Gowri Sankara Rao B.[2]

[1]Department of Chemistry, GITAM School of Science, GITAM Deemed to be University, Visakhapatnam-530045, Andhra Pradesh, India

[2]Department of Physics, M.R. College (A), Vizianagaram-535002, Andhra Pradesh, India

✉Corresponding Author: sganapav@gitam.edu

ABSTRACT

This research uses computational analytical tools to study the impact of nano-dopants on the characteristics of liquid crystals. The main focus of the study is on the conformation analysis and degree of interaction between liquid crystal materials and nano-dopants. FTIR, UV visible spectroscopy, and thermal microscopic techniques are among the spectroscopic methods employed to analyze the information. Furthermore, computationally driven approaches are used to gain a deeper understanding of how nano-dopants influence the characteristics of materials. The molecular interactions between the various functional groups of pure and nanocomposite materials can be investigated by utilizing the wavelet transform on FTIR spectrum data. Additionally, the presence and influence of nano-dopants on liquid crystals are investigated through polarized optical microscopy (POM) and correlation studies of optical texture analysis with UV visible spectroscopy. Here, p, n-alkoxybenzoic acid (nOBA, where n = 7,9) doped with magnetic nanoparticles (Fe_3O_4) of size 20nm is considered for investigation. The findings from this study show the successful utilization of computational methods to analyze the effect of nano-dopants on the characteristics of liquid crystals and their potential use in the development of biosensor devices.

Keywords: Nano-Doped Liquid Crystals, Nanoparticles, FTIR Spectroscopy, UV-visible Spectroscopic Technique, Wavelet Transform, Polarizing Optical Microscope, Absorbance.

RASĀYAN *J. Chem.*, Vol. 17, No. 1, 2024

INTRODUCTION

In recent decades, significant advancements have been made in the interdisciplinary development of Liquid Crystal (LC) materials. These advancements have led to the fabrication of various devices for other applications, including chemical and biological sensors.[1-4] Progress in this field has been achieved through the implementation of specific strategies, including the selection of appropriate chemical moieties with diverse molecular structures, shapes, and sizes, which are then mixed or doped into liquid crystal materials. These strategies have proven to be viable for device applications.[5-8] Liquid crystals (LCs) are characterized by specific thermo-optical, electric, magnetic, and dielectric properties that make them highly promising for a variety of applications. It is well known that LCs are good model systems for nanoparticle doping, a subject that many scientific and technical communities have diligently examined and successfully studied.[8-12] The dispersion or doping of nanoparticles in liquid crystalline materials gives rise to new supramolecular systems due to their self-assembling nature. The molecular interaction between the liquid crystalline material and nanoparticles at the surface often exhibits interesting and sometimes unexpected properties.[13,14] These properties, such as structural, molecular, thermo-optical, and electro-optical properties, can be tuned or modified from the initial compounds. The performance of the systems is improved by this type of tuning, which leads to a wide range of novel applications in optical devices, displays, biological devices, drug design, and medicine.[7,15-18]The current research utilizes magnetic nanoparticles (Fe_3O_4) with a size of 20nm as dopants, while p, n-alkoxybenzoic acid (nOBA, where n = 7,9) is used as the base material. The ability of liquid crystals to self-assemble facilitates the synthesis of supramolecular nanocomposites by doping Fe3O4 nanoparticles into p-n alkoxy benzoic acid, and they are represented as NnOBA, where n = 7,9. Magnetic nanoparticle doping of p-n-alkoxy benzoic acids significantly affects the liquid crystal's characteristics.[17,18] FTIR and UV visible spectroscopy and Polarizing Optical Microscope (POM) are used in the case of certain substances, such as nanodoped liquid crystals, to verify the existence of nanoparticles

http://doi.org/10.31788/RJC.2024.1718680

within the liquid crystals.[18-20] Here, computational approaches have been employed for the characterization of nanodoped liquid crystals. The increasing interest in computer vision for various scientific applications, as well as the ability of digital devices to respond to specific compounds, has made this possible.[21-24] The proposed computational approaches involve the wavelet transform of FTIR data and the correlation of optical texture analysis with UV-visible spectroscopy. These computational methods offer an objective and quantitative analysis of the techniques above. Fourier Transform Infrared Spectroscopy (FTIR) encounters challenges related to variable collinearity when the liquid crystal materials are doped or mixed with nanoparticles or dopants. Due to the similar vibrational frequencies of individual liquid crystals and nano-doped liquid crystals, it can be difficult to identify the functional groups involved in self-assembly processes that construct supramolecular structures.[19,25,26] Furthermore, varying transmitted intensities result in the absorption of radiation through unique vibration patterns of molecules within specific areas, such as the groups and fingerprint regions, which cannot be seen with the human eye. To ascertain the influence of nano-dopants on liquid crystalline materials, it is important to differentiate between the vibrational frequencies and absorption intensities of substances.

The FTIR wavelet transform is utilized to address this concern. This approach decomposes the spectral data into high- and low-frequency bands, which enable the analysis of FTIR spectra at different spatial resolutions.[21,27-29] The detection of variations in vibrational frequencies and variations in functional group intensities is made possible by the analysis of these subbands. Cross-correlation and structure similarity index measures are two varieties of similarity measures that are computed in this study from the subbands. These parameters have proven to be important in identifying the observed variations.[30-32] Polarizing optical microscopy (POM) is typically the initial method to determine the textures and phase transition temperatures of any new system.[33] In addition to phase transition temperatures, optical textures recorded from POM are useful for absorbance studies of samples through the computational technique known as optical texture analysis. This technique is correlated with UV-visible spectroscopy.[24,34,35]

The appearance of distinctive pattern textures with different shapes and colors is dependent on the nature and arrangement of molecules for their absorption wavelengths. Consequently, correlation studies of optical texture analysis with UV-visible spectroscopy provide information about the absorbencies of liquid crystals in the presence of nanoparticles and their influence on liquid crystalline properties. Results obtained from this study demonstrate that computational approaches are successful in investigating the influence of nano-dopants on the characteristics of liquid crystalline materials and their utility in the fabrication of biosensor devices.

EXPERIMENTAL

Chemical ingredients p,n-alkoxy benzoic acid (nOBA, where n=7,9), and Ferric oxide (Fe_3O_4) nanoparticles are brought from Sigma-Aldrich laboratories in the USA and used as such. The size of magnetite (Fe_3O_4) nanoparticles is 20 nm, and 0.5% in weight of the liquid crystalline material is considered for doping. These magnetite nanoparticles are introduced in the isotropic liquid phase of liquid crystal material (p,n- alkoxy benzoic acid) and they are continuously stirred for almost three hours. After cooling, the resultant nanodoped p-n alkoxybenzoic acids (nOBA) are subjected to study. For the preparation of the sample cell, an ITO-coated planar alignment cell with 5 μm thickness is taken into consideration.[36] Liquid crystal sample was inserted into the cell using capillary action for the experimental measurements. Once the sample cell was prepared, LCs were examined using the POM technique.

To observe and record the textures of the samples, a polarizing optical microscope - an SD-Tech with a hot stage and camera attachment is used.[33,37] ± 0.1°C is the accuracy of the temperature measurements used for studies. The recorded image has a resolution of 2816 x 1880 pixels and uses true color creation with 24-bit tonal values that fall between 0 and 255 grey levels. In the red, green, and blue monochromatic image planes, the optical textures of the samples are recorded separately.[38,39] The FTIR spectra of individual compounds and their complexes were recorded using an AGILENT CARY 630 Infrared Spectrometer.

A Lab India Analytical UV-visible spectrophotometer model UV-3092 was used to obtain the UV-visible spectra of pure and nano-doped liquid crystals. Computational analysis of pure and nano-doped liquid crystals has been carried out on the MATLAB platform.[40-42] The methodologies of the present investigation are explained in the following section.

Theory

Computational Methodology: Wavelet Transforms

A wavelet is a short waveform that enables simultaneous time and frequency analysis using versatile mathematical operations. The wavelet's mathematical functions are produced by the basic function given in Equation (1).[43-45]

Wavelet equation
$$\psi_{a,b}(t) = \frac{1}{\sqrt{|a|}}\psi\left(\frac{t-b}{a}\right) a,b \in R, a \neq 0 \quad (1)$$

This wavelet function has two parameters called scaling (a) and translation (b), which capture low and high-frequency information from the signal. Based on the applications, wavelet transform (WT) selects the frequencies. There are two distinct wavelet transforms: the Continuous and the Discrete such as CWT and DWT. In the past few years, DWT has had new applications in signal processing, image analysis, earthquake prediction, human vision, biosensors, drug designing etc.[27-29,46] Here also, DWT is considered for FTIR analysis. Discrete wavelets come in many different types, including Haar, Daubechies, Coiflet, Symlet, Biorthogonal, etc.[43-46] Based on the applications, appropriate wavelet functions are chosen for the analysis of signals or images. Here, the wavelet of Coiflet-5 is used for the analysis of FTIR spectral data. The waveform of the Coiflet-5 scaling and wavelet functions are shown in Fig.-1. The scaling and wavelet functions of DWT are related to low pass and high pass filters, and it decomposes the signal into approximation bands and detail bands. The FTIR wavelet transform can be thought of as a projection method, whereby FTIR spectrum data is projected into a collection of fundamental functions known as wavelets. The Coiflet-5 low pass and high pass filters were derived from the wavelet and scaling functions, and they are provided below.[47] Coiflet-5 wavelet - Low pass filter coefficients: [-0.00014996 0.00025356 0.0015402 -0.0029411 -0.0071638 0.016552 0.019918 -0.064997 -0.0368 0.29809 0.54751 0.30971 -0.043866 -0.074652 0.029196 0.023111 -0.013974 -0.0064801 0.004783 0.0017207 -0.0011758 -0.00045123 0.00021373 9.9378e-05 -2.9232e-05 -1.5072e-05 2.6408e-06 1.4593e-06 -1.184e-07 -6.73e-08]. Coiflet-5 wavelet- High pass filter coefficients are derived by reversing the order of the low pass filter coefficients and then reversing the sign of every second one.

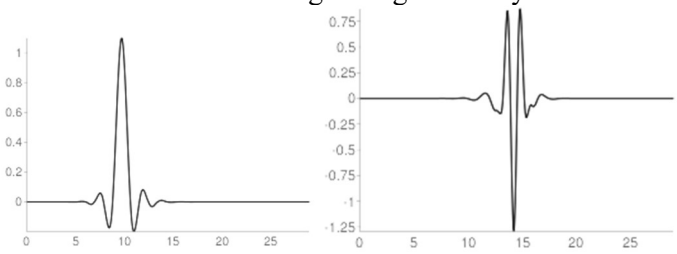

(a) (b)

Fig.-1: (a) Scaling Function (φ);(b) Wavelet Functions (ψ) of Coiflet-5

Figure-2 illustrates the steps needed in applying the Coiflet wavelet transform to the signal.

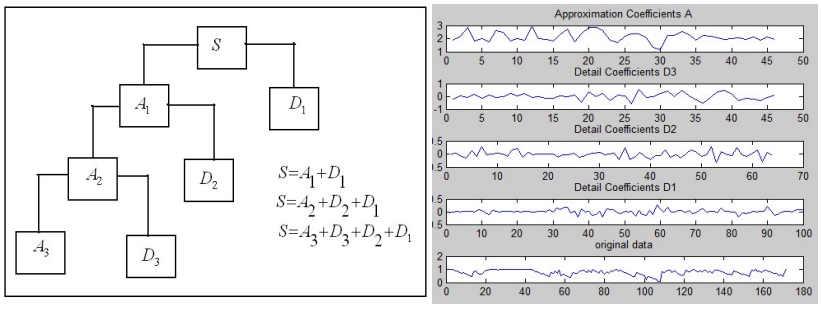

(a) (b)

Fig.-2: (a) Schematic Representation of Wavelet Decomposition at Level 3; (b) Structure of Wavelet decomposition of FTIR

Figure-2 shows how the data (*S*) is divided into high-frequency (detailed part) and low-frequency components (approximated part) when wavelet filters are projected onto it. The 3rd level decomposition of

the wavelet transform yields the 4 frequency subbands for a signal, such as the detail subbands (D1, D2, and D3), which contain high-frequency information, and the approximation band (A), which contains the low-frequency information.[30,43-49] This was shown clearly in Fig.-2. Once the multi-level decomposition of the FTIR spectra of the given samples is done, the subbands are used for further analysis based on the application. Here, the similarity measures computed from the subbands are used to identify the similarities and dissimilarities between two signals; the signal is the FTIR spectra. This was done by measuring cross-correlation parameters and structure similarity index at different details, and approximations using MATLAB. Equations related to the cross-correlation parameter and sequence scale parameter are given in.[30-32]

Optical Texture Analysis: Obtaining the Absorption Image

The optical texture (*I*) of the sample is recorded using POM under crossed and parallel polarizer conditions. Texture (*I*) is composed of 'm' pixels in the vertical direction and 'n' pixels in the horizontal direction. Its dimensions are m by n. The image's horizontal and vertical coordinates are denoted by *i* and *j*. m*n = N gives the total number of pixels in the image. The absorbance of each pixel of the optical texture is computed using equation (2).[50]

$$A(i,j) = -log_{10}\left(\frac{I(i,j) - I_{min}(i,j)}{I_{max}(i,j) - I_{min}(i,j)}\right) \quad (2)$$

Where '*A'* stands for absorbance of the sample, *I* represent the texture image recorded from the cross-polarization components of the sample, and in the absence of a sample the texture acquired from the parallel polarization components gives the I_{max}. When there is no sample, the texture I_{min} is recorded from the crossed polarization components. $I(i,j)$, $I_{max}(i,j)$, and $I_{min}(i,j)$ represent the intensity value of texture images at the coordinate position (i,j). The summation of absorbance at each pixel value gives the absorbance of the texture. These absorbencies are computed for three monochromatic image planes having wavelengths in the visible region, generally red, green, and blue.

RESULTS AND DISCUSSION

The impact of nanoparticles on the characteristics of liquid crystals is investigated through the application of wavelet transform FTIR, Polarizing optical microscope, and correlation studies of optical texture analysis with UV visible spectroscopy. In particular, the existence of nanoparticles in liquid crystals is examined to learn more about how they affect these materials' characteristics.

Wavelet Transform of FTIR

The FTIR spectra of pure and nano-doped p-n alkoxy benzoic acid (nOBA, where n=7, 9) are recorded at room temperature and are shown in Fig.-3.

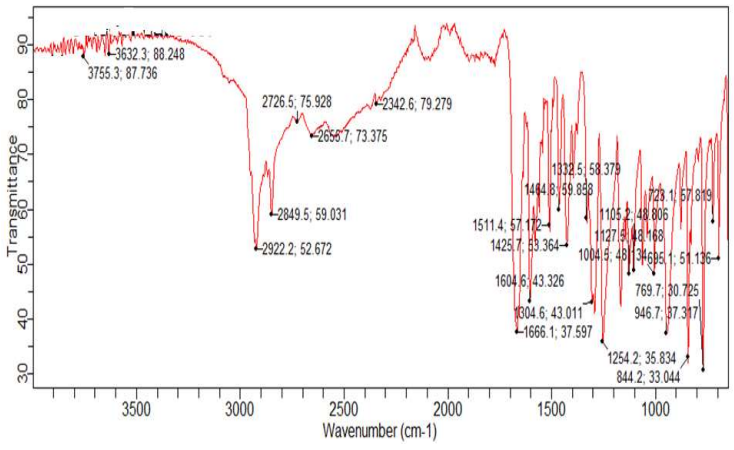

(a)

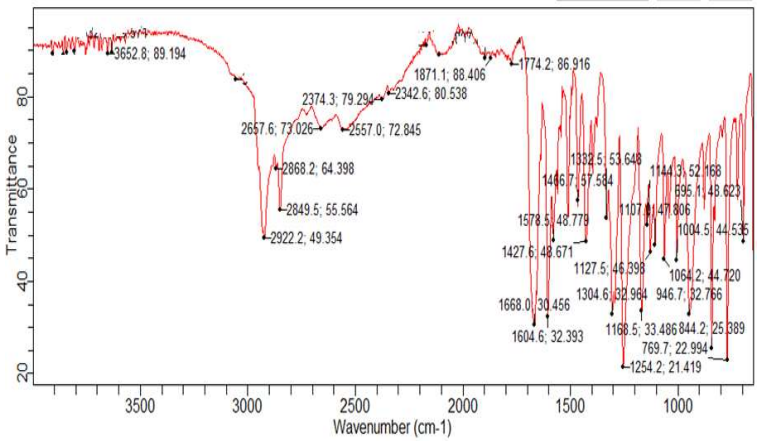

(b)

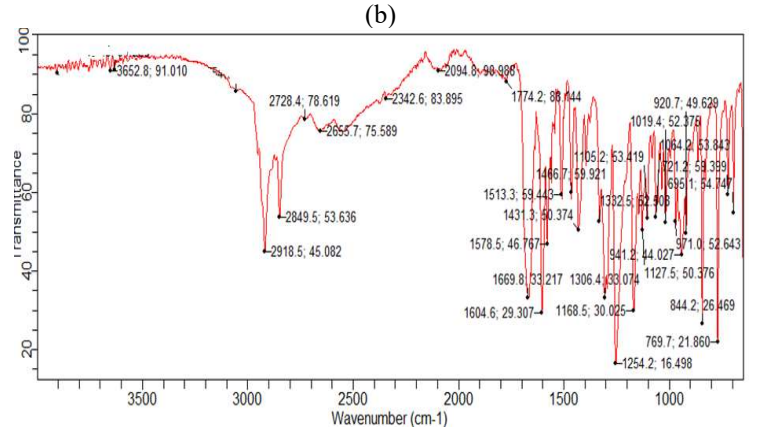

(c)

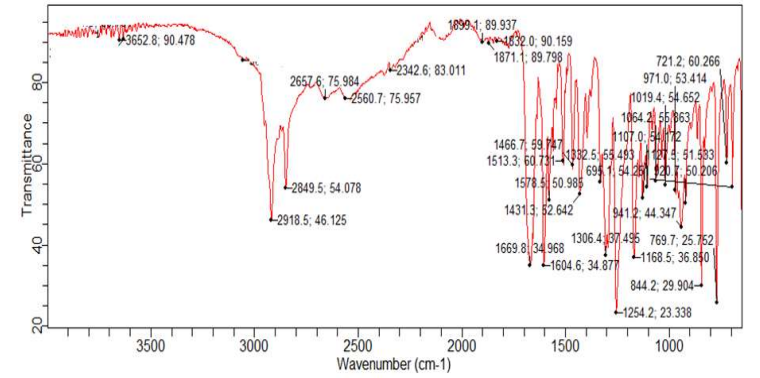

(d)

Fig.-3: FTIR Spectra of p-n Alkoxy Benzoic Acids (nOBA and NnOBA) (a) 7OBA; (b)9OBA; (c) N7OBA; (d) N9OBA

Based on the findings depicted in Fig.-3, it can be deduced that nanodoped liquid crystals (NnOBA) exhibit identical functional groups as their pure compounds (nOBA), with no discernible alterations or shifts in vibrational frequencies.[50] This implies a correlation between the vibrational frequencies of pure compounds and their nanocomposites. However, it is worth noting that the transmittances of radiation across all vibrational frequencies differ between nano-doped liquid crystals and pure liquid crystals (nOBA), as clearly demonstrated in Fig.-4. Figure-4 displays the overlapped FTIR spectra of 7OBA and N7OBA as an example case.

From the analysis of Fig.-4, it can be observed that similar to pure compounds, the functional groups present in the nanocomposites (NnOBA) also exhibit strong and intense absorption bands with reduced transmittance.[51] This reduction in transmitted intensity in the FTIR spectra can be attributed to changes in dipole moments that occur during vibration. The decrease in the transmitted intensities of stretching and

bending vibrations in the FTIR spectra confirms the presence and successful functionalization of nanoparticles in alkoxy benzoic acids.

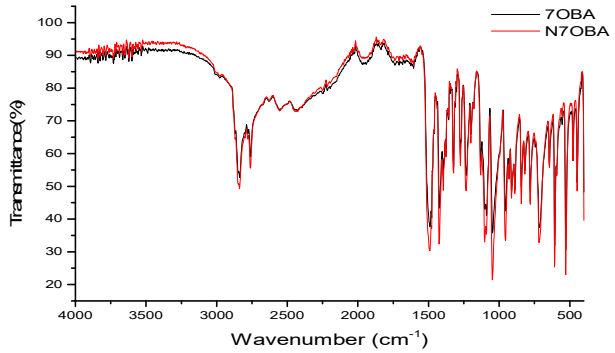

Fig.-4: Overlapping FTIR Spectra of 7OBA andN7OBA

However, the difference in transmittance radiation between pure compounds and nanocomposites in their respective regions is not discernible to the naked eye, as depicted in Fig.-4. Here, the computational approach of the wavelet transform of FTIR spectra was employed to identify variations in vibrational frequencies and differences in intensities of functional groups. This decomposition was done using the computational tool MATALB. Here, the FTIR spectra of nOBA and NnOBA (where n=7,9) were subjected to decomposition into distinct frequency bands. This decomposition was achieved through the utilization of Coiflet-5 wavelets, employing a decomposition level of 3. The decomposed spectra of the 7OBA and N7OBA samples are shown in Fig.-5.

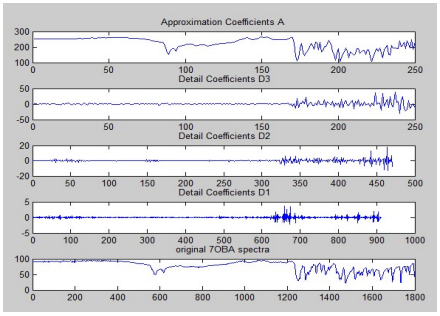

(a)

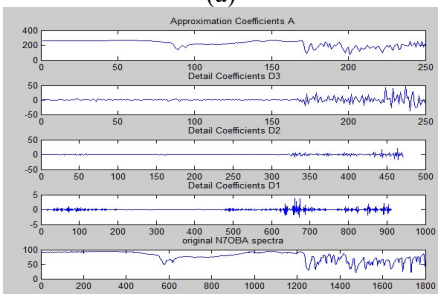

(b)

Fig.-5: Wavelet Transformed FTIR Spectra (a)7OBA;(b) N7OBA

Based on the findings presented in Fig.-5, it can be observed that the high frequency or noise information gradually separates into detail subbands (D1, D2, and D3), while the spectra remain within the discrete approximation band (A). The magnitude of the spectra within the detail subbands is significantly smaller in comparison to the discrete approximation, with minimal spectra present in these details. Consequently, the approximation band can be directly regarded as the filtered outcome. The spectra within the approximation subbands bear a closer resemblance to the original FTIR, as depicted in Fig.-5. Upon obtaining the multi-level decomposition of FTIR spectra of pure and nano doped liquid crystals, the cross-correlation parameter and structure similarity indices for the subbands are computed. These parameters are

measured between the subbands of 7OBA and N7OBA and 9OBA and N9OBA. Therefore, the influence of nanoparticles on liquid crystals can be identified. 100% correlation in both spectra is indicated by a cross-correlation coefficient value of +1, whereas 100% correlation in the opposite sense is indicated by a value of -1. Similarity measures computed for nOBA and Fe_3O_4 doped nOBA (NnOBA) where n=7,9 are given in Table-1.

Table-1: Similarity Measures of nOBA and NnOBA (where n=7,9)

Compounds	Similarity measures	Wavelet sub-bands			
		A	D1	D2	D3
(7OBA, N7OBA)	Cross-correlation	0.98	0.97	0.98	0.98
	Structure similarity	2.106	4.74	0.14	0.02
(9OBA, N9OBA)	Cross-correlation	0.99	0.98	0.99	0.99
	Structure similarity	2.42	4.87	0.15	0.02

From Table-1, it is observed that similarity measures between (7OBA, N7OBA) and (9OBA, N9OBA) are high for both compounds. The results indicate that there is a strong correlation between the pure and nano-doped liquid crystals of NnOBA (where n=7,9), suggesting that the impact of Fe_3O_4 nanoparticles on the nOBA liquid crystals is minimal. The interaction between the surface of the nanoparticles and alkoxy benzoic acids is small. However, the influence of nanoparticles is significantly greater in N7OBA compared to N9OBA. These deviations in properties from one compound to another may be attributed to increasing alkoxy chain length, molecular nature, and molecular size. Similar observations were made through the analysis of thermal and optical textures.

Optical Texture Analysis: Polarizing Microscope Studies

Phase transitions and optical textures of the p-n alkoxy benzoic acids and Fe_3O_4 doped liquid crystals NnOBA (where n=7,9) have been observed and recorded using polarized optical microscopy (POM). The compounds 7OBA and 9OBA exhibit the enantiotropic nematic and smectic C phases.[33] The dispersion of nanoparticles (Fe_3O_4) in the liquid crystals of nOBA results in the formation of self-assembled nanocomposites, namely N7OBA and N9OBA. The complexation of nOBA with Fe_3O_4 nanoparticles suppresses the smectic C phase of 7OBA and 9OBA and induces the smectic A phase in N7OBA and N9OBA, while the nematic phase remains unchanged. The textures of the pure and nanocomposites can be seen in Fig.-6. Table-2 lists the phases and corresponding transition temperatures for the pure and nano-doped materials.

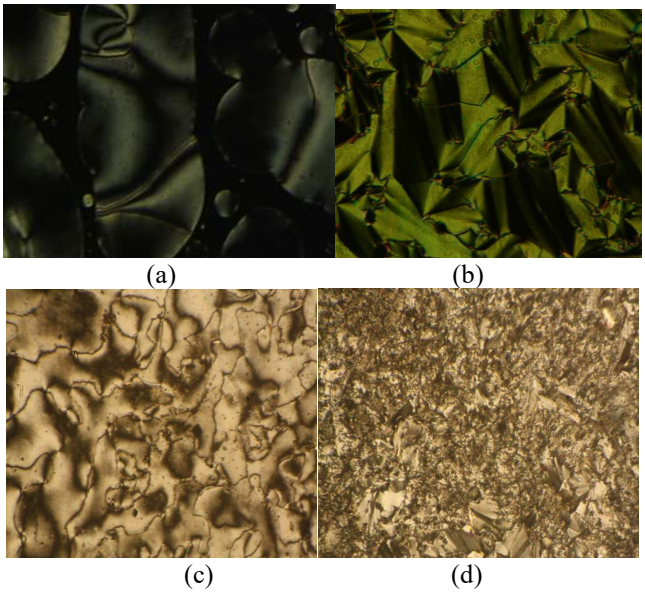

Fig.-6: Optical Textures of Liquid Crystalline Phases (a) Threaded Nematic Phase (b) Smectic C Phase of p, n-alkoxy Benzoic Acid (nOBA, where n=7,9); (c) Threaded Nematic Phase (d) Smectic A Phase of Nano Doped (Fe_3O_4) *p*, *n*-Alkoxy Benzoic Acid (NnOBA, where n=7,9)

Table-2: Phase Transitions and Transition Temperatures of *p*,*n*-alkoxy benzoic acid (nOBA) and nano doped (Fe_3O_4)*p*,*n*-alkoxy benzoic acid (NnOBA), where n=7,9.

Compounds	Phases	Phase transition temperatures (°C) POM
7OBA	I – N – Smectic C – Cr	146.0 – 98.0 – 92.0
9OBA	I – N – Smectic C – Cr	143.0 – 117.0 – 94.0
N7OBA	I – N – Smectic A – Cr	139.9 – 105.4 – 91.0
N9OBA	I – N – Smectic A – Cr	137.5 – 103.7 – 93.0

(Cr – Crystal, N- Nematic, I- isotropic)

According to the data presented in Table-2, it can be observed that the clearing or isotropic temperatures of nano doped liquid crystals have decreased in comparison to pure liquid crystals.[52] This reduction is thought to be caused by an increase in the van der Waals attraction between nanoparticles, which disrupts the director's orientational qualities in the liquid crystal medium. Consequently, strong anchoring conditions are formed among the nanoparticles, excluding the neighboring molecules, thereby influencing the molecular alignment of the liquid crystals and resulting in the formation of topological defects.[53,54] These topological defects are visually represented as new texture formations, as shown in Figs.-6(c) and 6(d). After numerous interactions within the liquid crystal medium, the nanoparticles appear to stabilize, leading to a weakening of the surface anchoring properties. These observations indicate that the elastic energy prevails over the magnetic energy when the orientation of the director is fixed.[55] Specifically, the nanoparticles affect the alignment of the liquid crystal molecules in the smectic C phase and attempt to induce layering, which is characteristic of the smectic A phase. Magnetic anisotropy is believed to be primarily caused by the aggregation of magnetite nanoparticles, as observed in the textures of the Smectic A phase as shown in Fig.-6(d). Since it overcomes the randomly aligned molecules with uniaxial symmetry in the liquid crystalline phases, its contribution is probably found on the particle surface. The influence of nanoparticles Fe_3O_4 on the nOBA liquid crystal was also studied from correlation studies of optical texture analysis and UV visible spectroscopy. Figure-7 displays the UV-visible spectra of samples that were taken at room temperature.

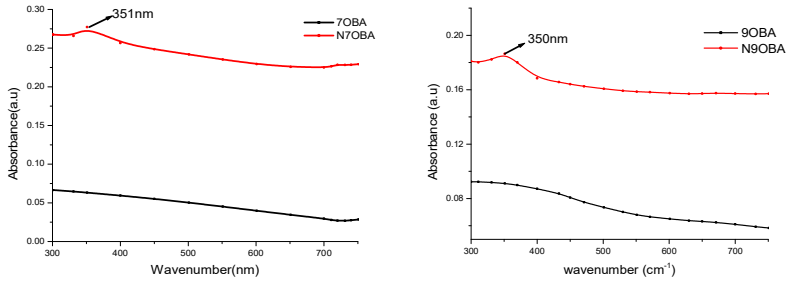

(a) (b)

Fig.-7: UV Visible Spectra of nOBA and NnOBA (where n=7,9)

UV-visible spectra of p-n alkoxy benzoic acids (nOBA) and nano-doped samples of NnOBA, where n=7,9, reveal that there are no absorption peaks visible in the 300–700 nm wavelength region for pure nOBA. The prepared nano doped liquid crystals' presence of Fe_3O_4 nanoparticles is further confirmed by the UV-visible spectrum analysis, as evidenced by the significant peak at 351 nm, which is a characteristic peak for the Fe^{3+} ion.[56,57] The absence of absorption peaks, except for the peak of the Fe^{3+} ion, suggests that the given liquid crystals are optically active and transparent materials for all wavelengths in the visible region. The same will be proven from the optical texture analysis. Once the textures of liquid crystals (nOBA and NnOBA) are recorded in true color form and at three monochromatic wavelengths,[38,58] the absorbance of the optical textures is computed from eq. (2) using the computational tool MATALB. Absorbance computation of liquid crystal texture is carried out at room temperature since UV-visible spectra of samples were recorded at room temperature. Optical textures and their optical absorbance images of p-n alkoxy benzoic acids and Fe_3O_4 doped p-n alkoxy benzoic acids at room temperature are shown in Fig.-8. As a representative case, the textures of 9OBA and N9OBA are shown.

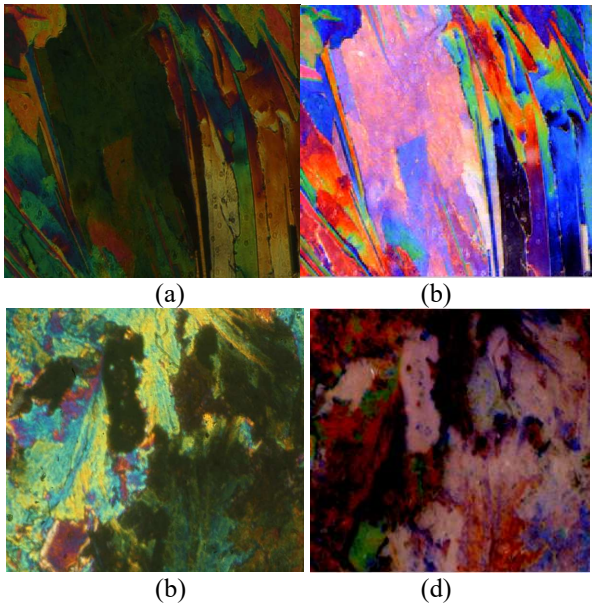

Fig.-8: Optical Textures and Their Optical Absorbance Images at Room Temperature (a and b) for 9OBA; (c and d) for N9OBA

The absorbance images displayed in Fig.-8 demonstrate that both pure and nano liquid crystals are transparent for all wavelengths not contained in the narrow transmission peak for a single wavelength. This is evidenced by the optical textures and absorbance images that appear with different color combinations. The dispersed nature of nanoparticles in liquid crystals affects the surface alignment of molecules. As a result, changes in textural features such as color, intensity, roughness, randomness, etc. Therefore, the transmitted intensities as well as the absorbencies of the optical textures of liquid crystals are modified. The absorbance image appears as a complementary image to the transmitted optical texture in true color form. In many cases, the optical effect (color change) as a function of concentration and temperature is measured using UV/Vis absorption spectroscopy, whereas, in liquid crystals, the optical effect as a function of external fields can be studied using optical texture analysis. As a result, the absorbency values derived from these images show a linear relationship with the actual absorbance values determined using UV/Vis spectroscopy at various visible spectrum wavelengths.[23,33,35] This was supported by measuring the monochromatic absorbencies measured at the wavelengths of 600nm, 540 nm, and 430nm from the optical texture analysis and UV visible spectroscopy. They are given in Table-3.

Table-3: Absorbencies at the Wavelengths of 600 nm, 540 nm, and 430 nm obtained from the UV Visible and Optical Texture Analysis

Wavelength (nm)	Techniques			
	UV visible		Optical texture analysis	
	7OBA	N 7OBA	7OBA	N 7OBA
600	0.04032	0.2303	0.2846	0.1283
540	0.03365	0.2134	0.1944	0.01421
430	0.06325	0.2517	0.4181	0.17783
	9OBA	N 9OBA	9OBA	N 9OBA
600	0.067	0.1453	0.5962	0.2802
540	0.058	0.1354	0.41068	0.1669
430	0.0865	0.1648	0.6147	0.352

From Table-3, it is clear that for all three wavelengths, the absorbance values of nanocomposites vary from the individual compounds in both techniques. In the UV-visible technique, absorbance increases from pure compounds, while in contrast, absorbance values decrease from pure compounds in optical texture analysis. These observations show clear signs of nanoparticle influence on the liquid crystals. Even though the parameters obtained from both techniques show increasing deviations in their absorbance values, they vary

linearly concerning the wavelength (shown in Fig.-9). Further, this is evidenced by the computation of sample absorbency correlation coefficients derived through the use of UV-visible and optical texture analysis techniques.

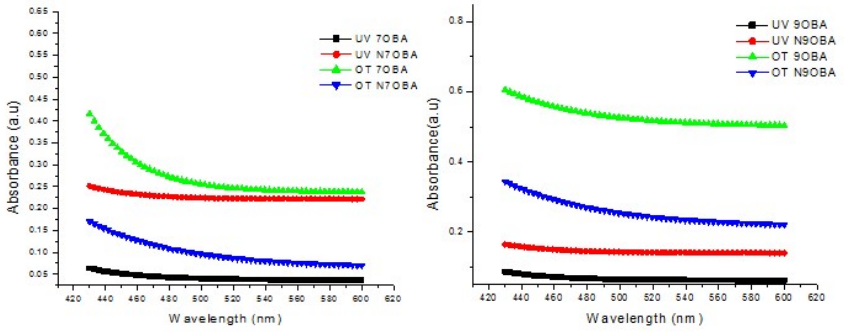

(a) (b)

Fig.-9: Absorbance Plots of UV Visible Spectroscopy and Optical Texture Analysis (a) for 7OBA and N7OBA; (b) for 9OBA and N9OBA

The present study reports on the correlation coefficients of absorbencies obtained from the UV-visible technique and optical texture analysis. The obtained values were 0.99839 and 0.98626 for pure 7OBA and 9OBA, respectively, and 0.96763 and 0.95254 for N7OBA and N9OBA, respectively. Notably, the correlation between absorbencies obtained from the UV visible technique and optical texture analysis was found to be stronger for 7OBA and N7OBA compared to 9OBA and N9OBA. These results indicate that optical texture analysis can provide precise measures of absorbencies that can be used as a trustworthy indicator of absorbing species as opposed to depending on absorbance values acquired using UV/Vis spectroscopy. This strategy can be very helpful for the creation of straightforward and affordable color-based sensors. The success of this correlation investigation can be attributed to the aptitude of optical sensors and probes to react to particular chemicals.[23,33,35] The results of the investigation used in this work have shown that nanoparticles are present in liquid crystals, and their presence significantly affects the molecular, thermal, and optical properties of these liquid crystals. Spectroscopic methods, including FTIR, UV-visible spectroscopy, and POM, as well as computational methods like wavelet transform and optical texture analysis, were used to explore these phenomena. It has been discovered that the characteristics of liquid crystal 7OBA, as opposed to 9OBA, are significantly influenced by the dispersion of Fe_3O_4 nanoparticles. This variance in attributes can be linked to elements such as the compound's size, quantity of carbon atoms, and molecular structure and arrangement. By studying the influence of nanoparticles on the characteristics of liquid crystalline materials, advancements can be made in the design and fabrication of devices for calorimetric applications. Alkoxy benzoic acids and their substituents are commonly used as antibiotics and preservatives in the pharmaceutical industry, and they exhibit parachromatic effects, where the color of the texture varies with temperature. Therefore, liquid crystal NnOBA holds promise for the development of devices for biological applications, such as biosensors, as the vibrational frequencies of the molecules and the color of the environment can provide information about diseased cells.[29,59,60]

CONCLUSION

The present study successfully investigates the confirmation and influence of liquid crystal properties in the presence of nanoparticles through the utilization of computational approaches such as wavelet transform FTIR and correlation studies involving optical texture analysis and UV visible spectroscopy. The presence of nanoparticles in p-n alkoxy benzoic acids is confirmed by the absorption peak of the Fe^{3+} ion at 351 nm, as well as the reduction in intensities of FTIR vibrational frequencies of functional groups. Furthermore, the alignment of molecules undergoes changes when the nanoparticle dispersion is introduced, resulting in modifications of the transition temperatures and optical texture (phase) changes of the liquid crystals. The computational studies employing wavelet transform and optical texture analysis techniques have provided novel insights into the design and fabrication of devices for calorimetric and biological applications straightforwardly and cost-effectively.

ACKNOWLEDGEMENTS

The authors are grateful to acknowledge M. R. College (A), Vizianagaram, A.P., The Gandhian Institute of Technology and Management (GITAM) deemed to be a University, Visakhapatnam, for providing special assistance to do research work.

CONFLICT OF INTERESTS

The authors declare that there is no conflict of interest.

AUTHOR CONTRIBUTIONS

All the authors contributed significantly to this manuscript, participated in reviewing/editing and approved the final draft for publication. The research profile of the authors can be verified from their ORCID ids, given below:

Sowmya M. https://orcid.org/0009-0005-5022-4306
Chandra Sekhara Rao G. https://orcid.org/0009-0004-8955-8672
Veera Raghava Sharma G. https://orcid.org/0000-0002-4550-0979
Srinivas Rao G. https://orcid.org/0000-0001-9647-7206
Gowri Sankara Rao B. http://orcid.org/0000-0002-7856-5816

REFERENCES

1. W. Iglesias, N. L. Abbott, E. K. Mann, A. Jakli, *ACS Applied Materials and Interfaces*, **4(12)**, **6884**(2012), https://doi.org /10.1021/am301952f
2. R. J. Carlton, J. T. Hunter, D. S. Miller, R. Abbasi, P. C. Mushenheim, L. N. Tan, and N. L. Abbott, *Liquid Crystals Reviews*, **1(1)**, **29**(2013), https://doi.org/ 10.1080/21680396.2013.769310
3. L. N. Tan, R. Carlton, K. Cleaver, N. L. Abbott, *Molecular Crystals and Liquid Crystals*, **594**,42(2013), https://doi.org/10.1080/15421406.2014.917470.
4. N. Popov, L.W. Honaker, m. Popova, N. Usol'tseva, E. K. Mann, A. Jakli and P. Popov, *Materials*, **11(20)**, 2(2017), https://doi.org/10.3390/ma11010020
5. G.R.Luckhurst and G.W. Gray, The Molecular Physics of Liquid Crystals, Academic Press, New York, USA(1979).
6. S.T. Ha, T.L. Lee, G. Y. Yeap, M. M. Ito, A. Saito, M. Watanabe, *Chinese Chemical Letters*, **23**, 177(2012), https://doi.org/10.1016/j.cclet.2010.09.017
7. O. Chaohai, D. Wang, *Advances in Civil Engineering*, **2021**, 1(2021), https://doi.org/10.1155/2021/5531679
8. R. A. Ramsey, S.C. Sharma, R. M. Henry, J.B. Atman, *Material Research SocietyProccedings,***771**, 339(2003), https://doi.org/10.1557/PROC-771-L10.18
9. I. C. Khoo, *Optics Letters*, **20(20),** 2137(1995), https://doi.org/10.1364/OL.20.002137
10. I. C. Khoo, Y. Z. Williams, B. Lewis, and T. Mallouk, *Molecular Crystals and Liquid Crystals*, **446,** 233(2006), https://doi.org 10.1080/15421400500377610
11. I. C. Khoo, A. Diaz, D. Kwon, D. H. Werner, *Journal of Nonlinear Optical Physics and Materials*,**16(3),** 381(2007), https://doi.org /10.1142/S0218863507003792
12. N. V. Kamanina, S. Likhomanova, Y. A. Zubtcova, A. A. Kamanin, *Journal of Nanomaterials,*2016, Article ID 8989250(2016), https://doi.org /10.1155/2016/8989250
13. C. Tschierske,*Chemical Society Reviews*, **36(12),** 1930(2007), https://doi.org /10.1039/b615517k
14. Y. Shiraishi, N. Toshima, K. Maeda, H. Yoshikawa, *Applied Physics Letters*, **81(5),** 2845(2002), https://doi.org /10.1063/1.1511282
15. G. Urban, Applications of Nanomaterials in Sensors and Diagnostics;Springer-Verlag, Heidelberg, Germany, **14**, (2013), https://doi.org/10.1007/978-3-642-36025-1

16. M. Ahmed, I. Saaem, P. C. Wu, A. Brown, *Critical Reviews in Biotechnology*, **34**, 180(2014), https://doi.org /10.3109/07388551.2013.778228
17. E. Kala , P. Vasanthi, S. Chitrarasu, M. Yogapriya, *Rasayan Journal of Chemistry*, **16**, 2091(2023), https://doi.org/10.31788/RJC.2023.1648494
18. W. X. Zhang, *Journal of Nanoparticle Research*, **5**, 323(2003), https://doi.org/10.1023/A:1025520116015
19. C.P. Sherman Hsu,2000, Infrared Spectroscopy,in: F.A. Settle (Eds.),In Handbook of instrumental techniques for analytical chemistry; Prentice Hall PTR: Upper Saddle River, NJ, pp. 247–283, https://doi.org/10.1080/10826079808006889
20. https://psiberg.com/uv-vis-spectroscopy/
21. R. Iranmanesh, A. Pourahmad, D. S. Shabestani, S. S. Jazayeri, H. Sadeqi, J. Akhavan and A. Tounsi, *Scientific Reports*, **13(1)**, 4266(2023), https://doi.org/10.1038/s41598-023-29898-x
22. T. Wang, L. Li, H. Yu-An, H. Zhang, M. Yahong and X. Zhou, *Molecules*, **23(4)**, 1(2018), https://doi.org/10.3390/molecules23040823
23. H. Araki, J. Kim, S. Zhang, A. Banks, K. Crawford, X. Sheng, P. Gutruf, Y. Shi, R. M. Pielak and J. A. Rogers, *Advanced Functional Materials*, **27(2)**, 1(2017), https://doi.org/10.1002/adfm.201604465
24. W. Xu-dong, O.S. Wolfbeis, *Analytical Chemistry*, **88(1)**, 203(2016), https://doi.org/10.1021/acs.analchem.5b04298
25. D. K. Ravish, S. Devi, S. G. Krishnamoo, N. R. Karthikeya, *Journal of Applied Sciences* **13(2)**, 207(2013), https://doi.org/10.3923/jas.2013.207.219
26. https://www.pharmtech.com/search?searchTerm=statistical%20outlier%20kmethod
27. A. Wakiuchi, S. Jasial, S. Asano, R. Hashizume, M. Hatanaka, O. Yu-ya, T. Matsubara, H. Ajiro, T. Sugawara, M. Fujii and T. Miyao, *ACS Omega*, **8(22)**, (2023), https://doi.org/10.1021/acsomega.3c01515
28. Akay M., Time Frequency and Wavelets in Biological Signal Processing, IEEE Press, New York, USA(1998).
29. X. Yang, Z. Wu, O. Quanhong, K. Qian, L. Jiang, W. Yang, Y. Shi and G. Liu, *Frontiers in Chemistry,* **10**, 1(2022), https://doi.org/10.3389/fchem.2022.810837
30. C.H.Trad,Qi Fang, I. Cosic, In proceedings of the 2nd conference of the Victorian chapter of the IEEE EMBS. Istanbul, TURKEY,25-Oct- 28-Oct,pp.115-119(2001).
31. Z. H. Almahdawie, Z. M. Hussain, *Journal of Theoretical and Applied Information Technology*, **96(24)**, 8399(2018).
32. https://in.mathworks.com/help/signal/ug/measuring-signal-similarities.html
33. D. Demus, L. Richter, Textures of Liquid Crystals, Verlag Chemie, New York, (1978).
34. D. Yusufu, A. Mills, *Sensors and Actuators B-Chemical*, **273**, 1187(2018),https://doi.org/10.1016/j.snb.2018.06.131
35. Y. Zhang, Y. Wu, Y. Zhang, A. Ozcan, Proceedings of SPIE, Optics and Biophotonics in Low-Resource Settings III, 28th Jan.- 2nd Feb., San Francisco, California, United States,(2017),https://doi.org/10.1117/12.2251537.
36. www.instec.com/pdf/brochures/LCCell-
37. S. Singh, Liquid Crystals Fundamentals, World Scientific, Singapore, (2002).
38. https://clarkvision.com/articles/
39. https://www.yumpu.com/en/document/view/45824597/digital-microscope-excel-technologies-inc
40. https://in.mathworks.com/products/matlab.html
41. Rafael C. Gonzalez, Richard Eugene Woods, Steven L. Eddins, Digital Image Processing Using MATLAB, Dorling Kindersley (India) Pvt.Ltd.,Delhi(2004).
42. C.J. Solomon, T.P. Breckon, Fundamentals of Digital Image Processing: A Practical Approach with Examples in Matlab, Wiley-Blackwell, Chichester, UK (2011).
43. K.P. Soman, K.I. Ramachandran, Insight into wavelets from theory to practice, Second Edition, Prentice Hall, India, Delhi (2006)
44. Martin Vetterli, Jelena Kovacevi, V.K. Goyal, The World of Fourier and Wavelets: Theory, Algorithms and Applications. Cambridge University Press, United Kingdom (2009).

45. Kamrul Hasan Talukder and Koichi Harada, *IAENG International Journal of Applied Mathematics,* **36**, 1(2007).
46. D. Shukla, J. Sahu, *International Journal of Electrical and Electronic Engineering & Telecommunications*, **4**, 30(2013).
47. X. Shao, W. Cai, *Reviews in Analytical Chemistry*, **17(4)**, 235(1998), https://doi.org/10.1515/REVAC.1998.17.4.235
48. R. Shriram, N. Daimiwal, *International Journal of Recent Technology and Engineering*, **8(4)**, 5647(2019), https://doi.org/10.35940/ijrte.D8527.118419
49. L. Inouri, S. Tighidet, M. Azni, A. Khireddine and K. Harrar, *Sensing and Imaging,***19(1)**, (2018), https://doi.org/10.1007/s11220-018-0212-0
50. http://www.prenhall.com/settle/chapters/ch15.pdf
51. https://chem.libretexts.org/Bookshelves/Physical_and_Theoretical_Chemistry_Textbook_Maps/Supplemental_Modules_(Physical_and_Theoretical_Chemistry)/Spectroscopy/Vibrational_Spectroscopy/Infrared_Spectroscopy
52. S. S. Sastry, S. Begum, T. V. Kumari, V. R. K. Murthy, S.T. Ha, *E-Journal of Chemistry*, **9(4)**, 2462(2012), https://doi.org/10.1155/2012/878049.
53. H. Stark, *Physics Report*, **351(6)**, 387(2001) https://doi.org/10.1016/S0370-1573(00)00144-7.
54. R. W. Ruhwandl, E. M. Terentjev, *Physical Review A, Atomic, molecular, and optical physics*, **55(3)**, 2958(1997), https://doi.org/10.1103/PhysRevE.55.2958.
55. F.Yeung,Y.L. J.Ho, Y.W. Li, andH. S. Kwok, *Journalof Display Technology*, **4(1)**, 24(2008), https://doi.org/10.1109/JDT.2007.900929
56. Y. Wei, S. Han, D. A. Walker, S. C. Warren, B. A. Grzybowski, *Chemical Science*, **3(4)**, 1090(2011),https://doi.org/10.1039/C2SC00673A
57. S. H. Chaki, T. J. Malek, M. D. Chaudhary, J. P. Tailor, and M. P Deshpande, *Advances in Natural Sciences: Nanoscience and Nanotechnology,* **6(3)**, 1(2015), https://doi.org/10.1088/2043-6262/6/3/035009
58. https://www.opsweb.org/page/Monochromatic
59. Ping-Yuan Lin, Yi-Wei Chung. Er-Yuan Chuang. Yen-Chieh WangMin-Chih Lai, Yen-Chin Hsu, Chun-Che Lin.Yu-Cheng Hsiao, *Frontiers in Bioengineering and Biotechnology,*11, (2023), https://doi.org/10.3389/fbioe.2023.1148446
60. Su, L. Wai-Leng, Cancers, **12(115)**, 1(2020), https://doi.org/10.3390/cancers12010115

[RJC- 8680/2024]